

RESEARCH ARTICLE

Fabrication and modeling of nanocomposites with bioceramic nanoparticles for rapid wound healing: An experimental and molecular dynamics investigation

Somayeh Tavasolikejani¹, Ashkan Farazin^{2*}

¹ Isfahan University of Technology, Department of Chemistry, Isfahan, Iran

² Department of Solid Mechanics, Faculty of Mechanical Engineering, University of Kashan, Kashan, Iran

ARTICLE INFO

Article History:

Received 25 Apr 2023

Accepted 10 Jul 2023

Published 01 Aug 2023

Keywords:

Hydroxyapatite

Polycaprolactone

Freeze-drying technique

Scanning electron

microscopy

Molecular dynamics

simulation

Simulated body fluid

ABSTRACT

In the present study, Fabrication and modeling of nanocomposites with bioceramic nanoparticles for rapid wound healing with (0wt. %, 5wt. %, 10wt. %, 15wt. % NPs) were investigated. After the fabrication of nanocomposites using the freeze-drying technique, X-ray diffraction (XRD) test is performed to show the crystallinity of hydroxyapatite and titanium oxide. Scanning electron microscopy (SEM) tests are performed to demonstrate the morphology of the structure, atomic force microscope (AFM) test is performed to show surface roughness and pores. Finally by placing nano scaffolds in a simulated body fluid (SBF) for 21 days, their weight and pH changes are measured. Then, by performing the tensile test, the results related to the tensile strength of the scaffolds are examined. In this paper, the sum of mechanical and physical laboratory results are compared with the results obtained by molecular dynamics simulation (MDs). The results show that with the increase of titanium nanoparticles, the physical and mechanical properties, as well as the healing properties of the wound dressing, have increased significantly. Also, the comparison of laboratory results and MDs results determine the accuracy of this method. Therefore fabricating these nanocomposites helps a lot for rapid wound healing.

How to cite this article

Tavasolikejani S., Farazin A. Fabrication and modeling of nanocomposites with bioceramic nanoparticles for rapid wound healing: An experimental and molecular dynamics investigation. *Nanomed Res J*, 2023; 8(4): 412-429. DOI: 10.22034/nmrj.2023.04.010

INTRODUCTION

Tissue engineering is the combination of cells, materials engineering techniques, and biochemical agents suitable for the improvement or replacement of biological tissues [1–3]. Tissue engineering involves the use of scaffolding to create novel tissue for a medical purpose [4]. Tissue engineering is a multidisciplinary field of principles and applications of engineering methods and life sciences [5,6], to fundamentally understand the relationship between structure and function in natural and diseased tissues [7–9]. Tissue engineering is a combination of cells, materials, and appropriate physical and chemical agents, which aim to maintain tissue balance or

improve the function of the target tissue or replace the biological function of the tissue [10,11]. Today, there is a great ability to make artificial organs and tissues so that the transplanted tissue and organ grows with the recipient after the transplant [12]. With this method, there is a permanent solution for treating damaged tissues [13–15]. So that there is no need for complementary therapies, and as a result, the cost of treatment is greatly reduced [16–18]. So far, tissue engineering has been used to repair many tissues, such as bone, cartilage, blood vessels, and skin [19,20]. Therefore, a texture needs a series of structural and mechanical properties to perform its function [21]. Biological scaffolds are made using biocompatible and degradable materials. The structure of the scaffold

* Corresponding Author Email: a.farazin@grad.kashanu.ac.ir

is porous, which helps the cells to adhere better [22,23]. The size and intensity of the porosity can be controlled. It should be said that the main part of the work is the design of the scaffold, in which the size of the cavities, the porosity intensity, and the degree of degradability are determined [24]. Naton et al. [25] researched hip prosthesis. They applied it in 3D with a coating of cartilage cells. The prosthesis was then replaced in the patient's body. Also, many articles have been done by MDs method. Haghighi et al. [26] investigated the effect of defects of carbon nanotubes (CNTs) on the mechanical behavior of nanocomposites with the cross-linked matrix of epoxy resin by MDs. They observed a change in the modulus of elasticity, especially a decrease in shear modulus when using defective nanotubes. Montazeri et al. [27] studied the effect of CNT orientation on the shear deformation properties of composite polymers by a combination of molecular dynamics and finite element methods. At 45° orientation, single-walled carbon nanotubes had the greatest effect on increasing the shear modulus. Mortazavi et al. [28] examined the mechanical properties and thermal conductivity of carbon nitride graphite nanoplates by MDs and recommended the use of this material in combination with polymers to enhance the mechanical properties. Ju et al. [29] studied the structure and mechanical properties of carbon fiber-based polypropylene nanocomposites by molecular dynamics method and comparison with the results of experimental measurements. Frankland [30] investigated the stress and strain behavior of polyethylene-based composite nanotubes by adding single-walled and multi-walled carbon nanotubes by MDs and observed an increase in stiffness relative to the polymer at long lengths of CNTs. Marcadon et al. [31] used a molecular and micromechanical dynamics approach to investigate the effect of nanoparticle size on the properties of polymer nanocomposites. In their research, silica nanoparticles in polymer and MDs simulation were used. The results showed that the modulus of elasticity of the composite

is very variable with respect to the particle size (silica) and the effective modulus increases with increasing particle size. Han et al. [32] considered the glass transition temperature and mechanical properties of polyethylene and PET / Silica, PET / Hydroxylated silica nanocomposites by MDs. And witnessed an increase in mechanical properties such as Young's modulus and Bulk modulus with increasing silica nanoparticles. Baljon et al. [33] have investigated the phenomenon of fragmentation in the breakdown of polymers by simulating MDs. The results of their study showed that if the length of polymer chains is longer than the length required for the complexity of the chains, the phenomenon of fragmentation occurs. This can be very important in enhancing the fracture toughness of polymers in which cracking occurs. Nackier et al. [34] studied the properties of titanium oxide and its modeling by MDs. Zhang et al. [35] studied the interaction and reaction and equations between the polymer and the hydroxyapatite reinforcement and used the MDs method to simulate it. The first clinical trials on hydroxyapatite and bone implants were performed by Forlong [36]. And after 10 years, only 2% of failure was reported for these implants. The main purpose of this study is to fabricate a polymer-based nanocomposite to help repair bone fractures. Then, using the MDs method, the prediction of mechanical and physical properties of simulated nanocomposites is performed. The laboratory results are used to validate the results of the MDs method.

MATERIALS AND METHODS

In this paper, biocompatible polymer PCL is used as the matrix, and HA and TiO₂ nanoparticles are used as reinforcements. It should be noted that dimethylformamide (DMF) solvent is used to prepare the polymer base fluid as shown in Table (1). DMF is a common solvent in chemistry. It is a polar solvent with a high boiling point. DMF is not stable against bases and strong acids and can be mixed in water in any proportion.

Table 1. Experimental pure materials for fabricating nanocomposites

Materials	Chemical formula	Manufacturer
HA nanopowder	Ca ₅ (PO ₄) ₃ (OH)	Merck - Germany
Titanium oxide	TiO ₂	Merck - Germany
PCL	(C ₆ H ₁₀ O ₂) _n	Aldrich - United states
DMF	C ₃ H ₇ NO	Merck - Germany



Fabrication and preparation of nanocomposite scaffolding

This experiment is performed to fabricate four samples each sample is considered 8g (6g as matrix and 2g as reinforcements), first to prepare a solution, 0.4g of PCL is added to 30 ml of DMF. It is then placed on a magnetic stirrer for 30 minutes to deform the solution into a jelly state. To fabricate the first sample (0.wt % TiO_2), 2g of HA is combined with 6g of the solution. To fabricate the second sample (5 wt. % TiO_2), mix 0.4g of TiO_2 with 1.6 g of HA and mix together for 180s, then combine with 6 g of the solution. To fabricate the third sample (10 wt. % TiO_2), mix 0.8g of TiO_2 with 1.2 g of HA and mix together for 180s, then combine with 6 g of the solution. To fabricate the fourth sample (15 wt. % TiO_2), mix 1.2 g of TiO_2 with 0.8 g of HA and mix together for 180s, then combine with 6 g of the solution. All 4 samples are placed on a magnetic stirrer for 30 minutes and poured into a petri dish, then placed in the freezer at -65°C for 40 hours.

Fabricating composite scaffolding with freeze drying technique

After removing the emulsion from the freezer, the completely frozen samples are placed in a freeze-dryer. Porous scaffolding was fabricated in

a freeze-drying machine for 20 hours at -45°C and a pressure of 0.03 millibar. After 20 hours, the scaffolds were removed and prepared for various experiments as shown in Fig (1).

With this method, nanocomposite scaffolds with different percentages of ceramic phase were fabricated. After fabricating the nanocomposites, XRD test is performed to show the crystallinity of HA and TiO_2 . SEM tests are performed to demonstrate the morphology of the structure. Finally, AFM test is performed to show surface roughness and pores. Schematic of all steps for fabrication nanocomposites is shown in Fig (2).

Investigation of structure and phase determination by XRD

In order to determine the phases in the synthesized powder and composite scaffolding, XRD test is performed with PHILIPS PW3040 device located in Kashan University in the range of 2θ between 10 to 90 degrees under 40 kV and 30 mA

Morphology and sediment formation of composite scaffolds using SEM

In order to study the size and morphology of the holes and porosities in the scaffold, a model SEM (AIS2100) from South Korea located in the

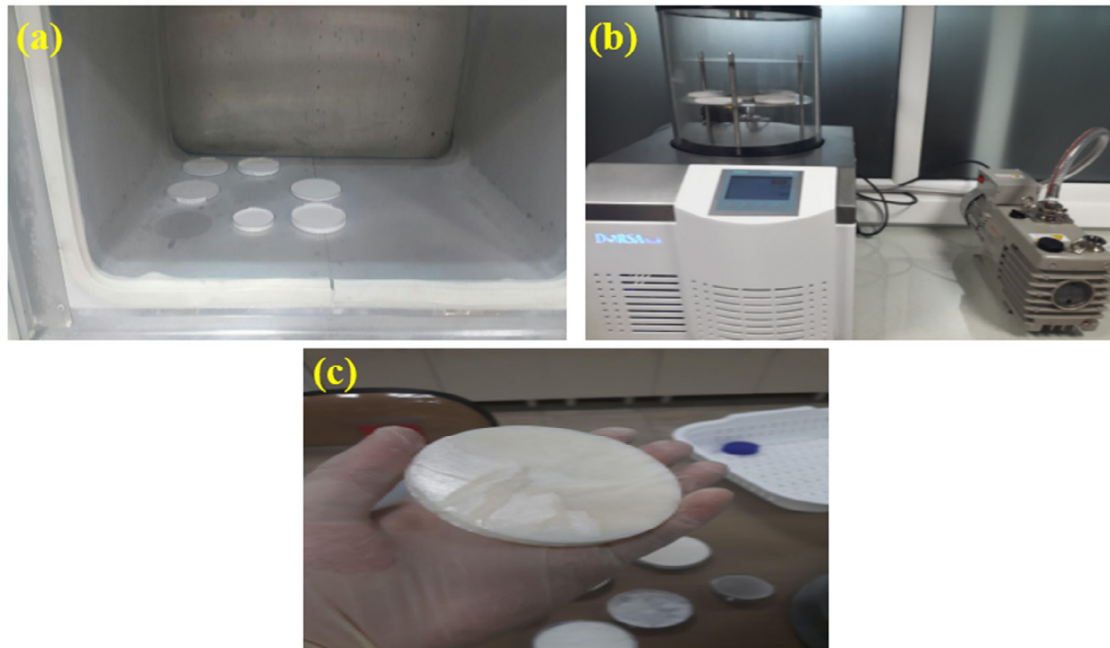


Fig. 1. Nanocomposite fabrication steps (a): Keep scaffolds in the freezer (40hr at -65°C) (b): After 40 hr., put scaffolds in the freeze dryer (20h at -45°C) (c): Novel scaffolds were fabricated by freeze drying technique

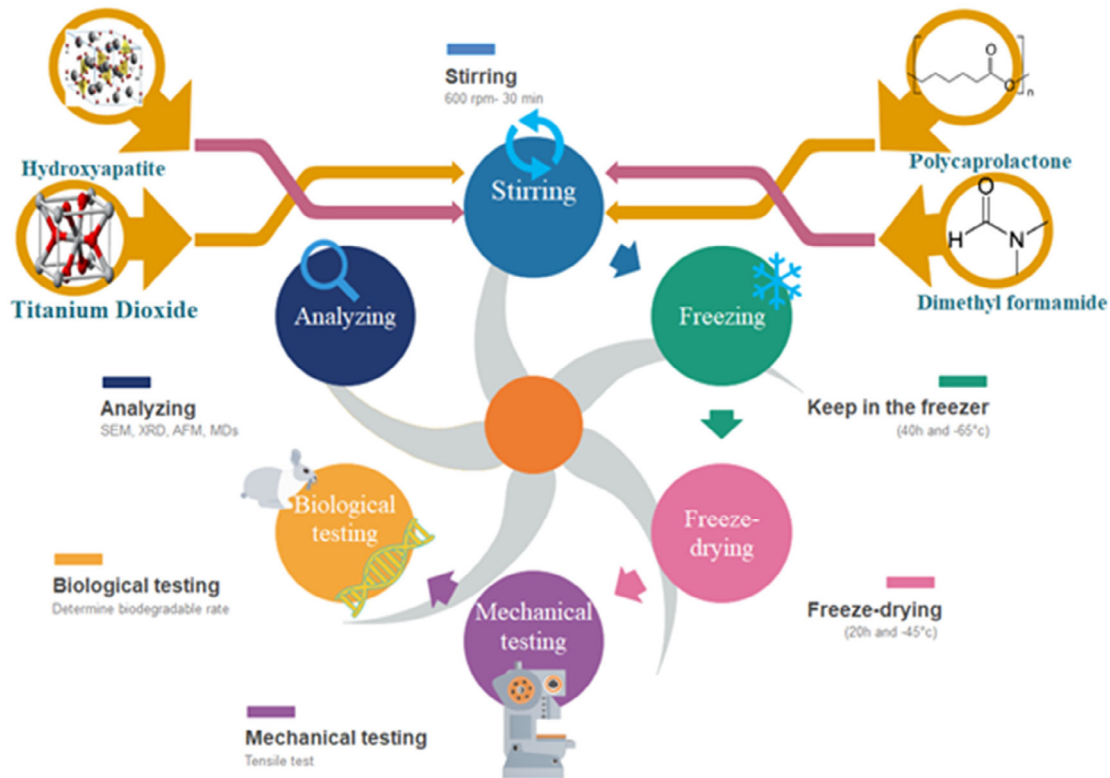


Fig.2. A visual representation is provided to showcase the step-by-step procedure of creating PCL-HA-TiO₂ nanocomposite scaffolds using the freeze drying technique

central laboratory of Amirkabir University is used. In order to increase the electrical conductivity of the sample surface and increase the clarity of the images, a thin layer of gold was sprayed on the samples before imaging. Thin layers were prepared from the side sections of the scaffolds and examined using the above device.

Structural study using AFM spectroscopy

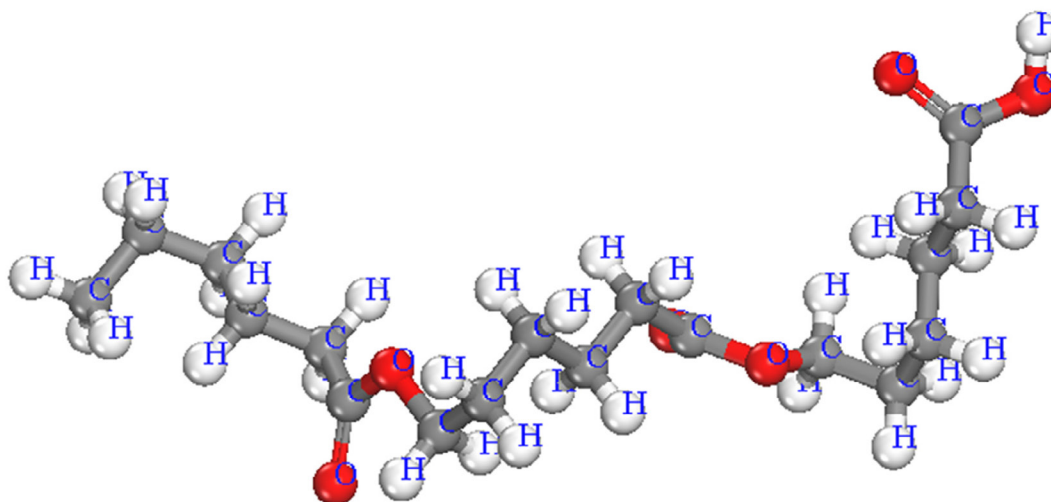
AFM, like scanning tunneling microscopes, are subsets of scanning probe microscopes. This microscope uses a very sharp tip to probe and map the elevation of the sample surface. AFM detects field forces close to each other between probe tip atoms and sample surface atoms instead of tunnel current. Because atomic force microscopy is not limited to electrical conductor surfaces, it is more widely used than scanning tunneling microscopes. It should be noted that to perform this test, an ENTEGRA AFMNT-MDT device made in the United States located at the University of Isfahan is performed.

Mechanical tests

To calculate the mechanical properties, Tensile strength test with (SANTAM machine) made in Iran is employed. For this purpose, each cube sample with a length and width of 30 mm and a thickness of 10 mm is prepared and loaded at a rate of 0.2 mm/min. The output of the device was in the form of force and displacement data. With the initial diameter and length of each sample, it became stress and strain. Finally, using the slope of the elastic region of the strain stress diagram, the elastic modulus of each sample is obtained. Mechanical behavior of nanocomposite scaffolds including compressive strength and elastic modulus using compressive strength test according to standard (ASTM-20) by the device (SANTAM-STM50) with pressure rate (0.5 mm/min) in the Institute of New Technologies, University of Technology Amirkabir is examined.

Measurement absorption of PBS and SBF

Biological evaluation of samples made

Fig.3. A polymer chain of PCL ($C_6H_{10}O_2$)

according to the relevant standard is performed in physiological solution. The porosity of each sample is measured according to the Archimedes principle to compare the dissolution rate of nanocomposite scaffolds. Also, the biological characteristics of the four different samples are analyzed by placing them in simulated body fluid (SBF) and phosphate buffer salt (PBS) for 21 days according to the description described by Kokubo et al. [37] Weight change, absorption rate and change in pH value of each sample are measured. For this purpose, scaffolds made with different percentages of polymer and ceramic phases are cut ($0.5 \times 1 \times 1$ cm) and weighed and then immersed in SBF at 37°C in a water bath. The scaffolds are then removed from the solution until they reach equilibrium. Based on the following equation (1), the percentage of water absorption is calculated [38].

$$\text{Swelling Ratio} = \frac{W_2 - W_1}{W_1} \times 100 \quad (1)$$

where W_2 and W_1 are the weights of each sample associated with the swollen and dry conditions, respectively.

Molecular structure of PCL, HA, and TiO_2

PCL is a biodegradable thermoplastic polymer obtained by chemical synthesis from crude oil. PCL is well resistant to water, oil, solvents, and chlorine. It also has a low melting point ($58\text{--}60^\circ\text{C}$) and low viscosity and is easy to process [39]. PCL is important

in medical use due to its very low melting point, biocompatibility, and high biodegradability. Due to its very low melting point, biocompatibility, and high biodegradability [40]. The chemical formula of PCL is $(C_6H_{10}O_2)_n$ in which 6 carbon atoms, 10 hydrogen atoms, and 2 oxygen atoms are joined together to form a polymer chain as shown in Fig (3). HA with the formula $Ca_3(PO_4)_3(OH)$ with a molecular weight of 31.502 has 89.38% calcium and 5.18% phosphorus. The structural texture of HA is very similar to the structural texture of bone [41]. Fig (4) shows the crystal structure of HA. Titanium is one of the most common metals on Earth, but it does not occur naturally in this primitive form. Titanium dioxide - Also called Titanium Oxide (IV), it is a compound that occurs naturally when titanium reacts with oxygen in the air. Titanium is found as an oxide in the earth's crustal minerals. It is also found with other elements such as calcium and iron. Its chemical formula is TiO_2 , which means that it is composed of one titanium atom and two oxygen atoms [42–44].

Simulation methodology: MDs Simulation steps, Force field, and Software

Molecular dynamics is a technique that can be used to determine the equilibrium state of a multi-particle system and also to calculate the desired properties of this system. MDs is actually a way of chasing particles or atoms. This method creates a history of a multi-particle system by numerically integrating Newtonian equations of motion. In MDs, it is assumed that these particles or atoms are

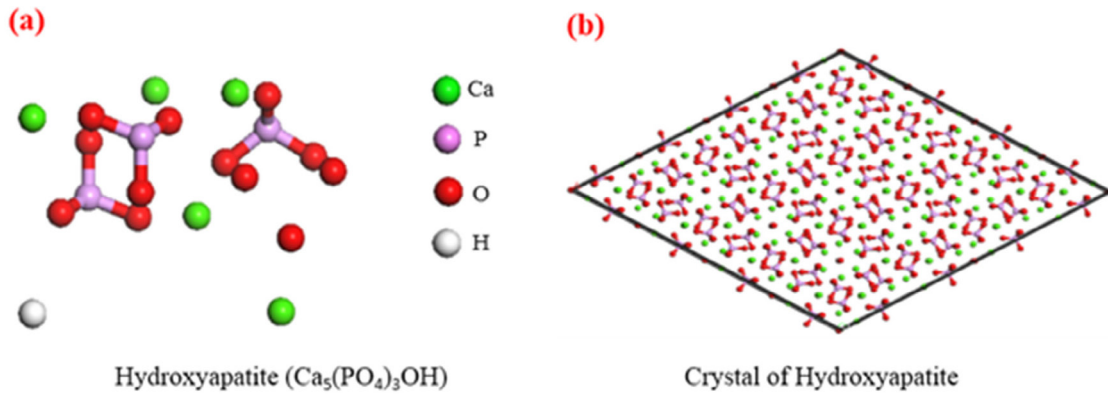


Fig.4. HA structure (a) atoms of HA (b) crystal structure of HA

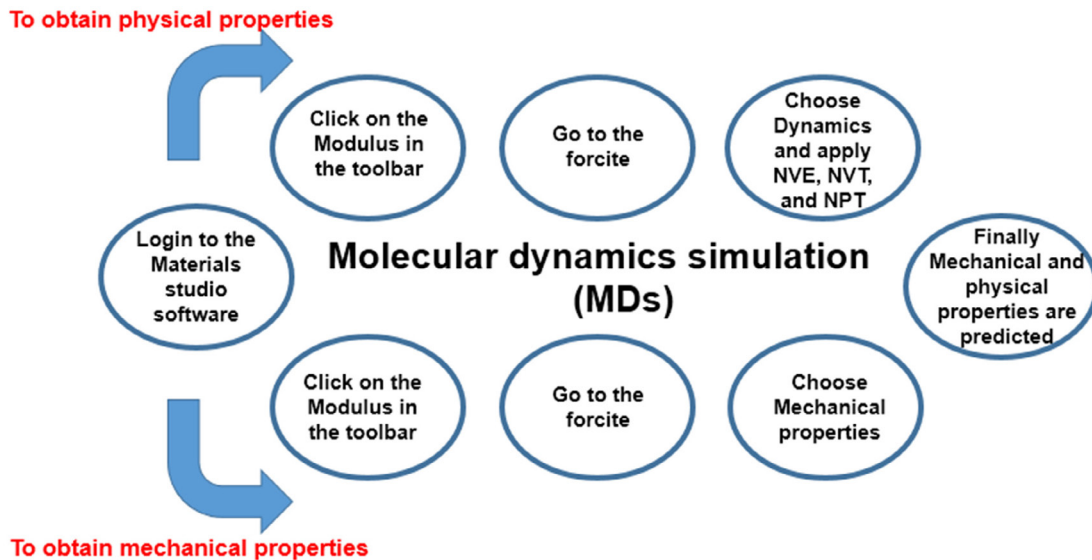


Fig.5. Four steps to predict mechanical and physical properties by MDs method

affected by the interatomic force field. The history of the motion of particles or atoms is determined in such a way that the continuity of the atoms relative to each other is optimal in the least energy. All the properties of simulated nanocomposites, including the mechanical properties such as the elastic property, are due to this interatomic or molecular force. As observe in Fig (5), the main following steps have been taken to complete the MD simulation. The initial atomistic models are simulated in Materials Studio software and Condensed-phase Optimized Molecular Potentials for Atomistic Simulation Studies (COMPASS) force field is determined for modeling inter and intra-atomic interactions. The COMPASS force field has extensive coverage in covalent molecules including

most common organic and small inorganic molecules. For obtaining mechanical and physical properties some ensembles (NVE, NVT, and NPT) must apply and define as follows [45,46]:

The ensemble of NVE reveals that the sum of kinetic (KE) and potential energies (PE) is conserved, T and P are unregulated and N, V, and E denote a constant number, volume, and energy, respectively. At this step, the simulation box is placed at a temperature of 300 K under NVE. The simulation time is considered 50 ps. The purpose of NVT is to increase the energy of the system so that the atoms have the energy needed to move towards equilibrium. In other words, the reason for the ensemble of NVT is the release of the molecular structure from the initial internal stresses that were

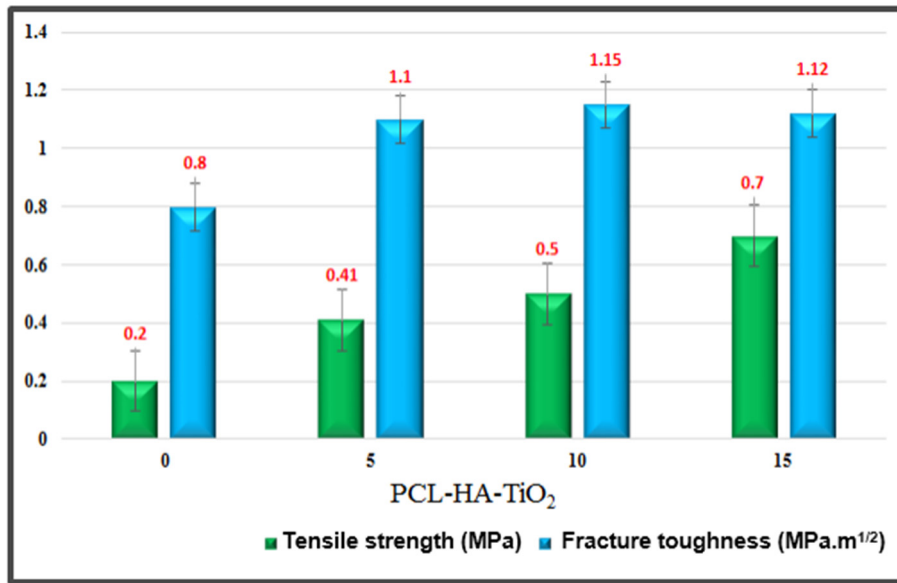


Fig.6. Tensile strength and fracture toughness diagram of PCL-HA-TiO₂

applied during the construction of the simulation box. Initial density of the system (0.9gr / cm³) is assumed to allow molecules and atoms to be displaced to move towards optimal mode and the simulation time considered 50 ps.

The reason for the ensemble of NPT brings the system density closer to the actual density. Also, NPT can eliminate system residual stresses. At this point, the system is pressurized at atmospheric pressure 1 at a temperature of 298 K under a constant NPT to close the system density to the actual density. It is worth noticing the simulation time at this stage considered 50 ps. At all stages to create simulated nanocomposite boxes, energy is minimized and optimized so that molecules and atoms can be placed at the best distance.

RESULTS AND DISCUSSION

In this section, after the fabrication of PCL- HA -TiO₂ bio-nanocomposite scaffolds with different weight percentages, the porosity and distribution were examined by SEM. XRD was performed to identify fuzzy and grafted. Water absorption was measured by swelling and immersion test by Kokubo method [37]. Then, by performing the tensile test, the results related to the tensile strength of the scaffolds were examined and structural analysis was performed. In the experiment as shown in Fig (6), the tensile strength increases with increasing the weight percentage of TiO₂ to the PCL

and HA (ceramic-polymer base). This increase is from 0.2 MPa to 0.7 MPa, which shows a growth of more than 3 times, and the fracture toughness increases up to 10 wt. % of TiO₂. In the experiment, by increasing the weight percentage of TiO₂ to the ceramic-polymer base of PCL-HA, the hardness of the composite increases due to the inherent nature of titanium. Therefore, the hardness for the sample of 0 wt. % of TiO₂ is about 0.9 (KgN / m²) and for the 15 wt. % of TiO₂ is about 3.4 (KgN / m²), which increases more than 3 times as shown in Fig (7). Also in Fig (7), Young's modulus increases with increasing TiO₂, which is about 36 MPa for 0 wt.% of TiO₂, and about 69 MPa for 15 wt.% of TiO₂, which shows a double increase.

The ability to form HA on the scaffold, which contributes to the proper interaction of cell and scaffold in order to produce bone tissue and the process of calcification of bone during its reconstruction, which can be expected to have good biocompatibility properties at the site of scaffold contact with tissue. Fig. (8) shows that with the increase of TiO₂ nanoparticles, the growth of HA increases 3 times. Also, the dissolution rate by experimental investigation shows that the sample of 0 wt. % of TiO₂ has the highest dissolution rate. According to Fig (8), the 0 wt. % TiO₂ sample is almost completely disintegrated, while the 15wt. % sample remains completely intact in the solution.

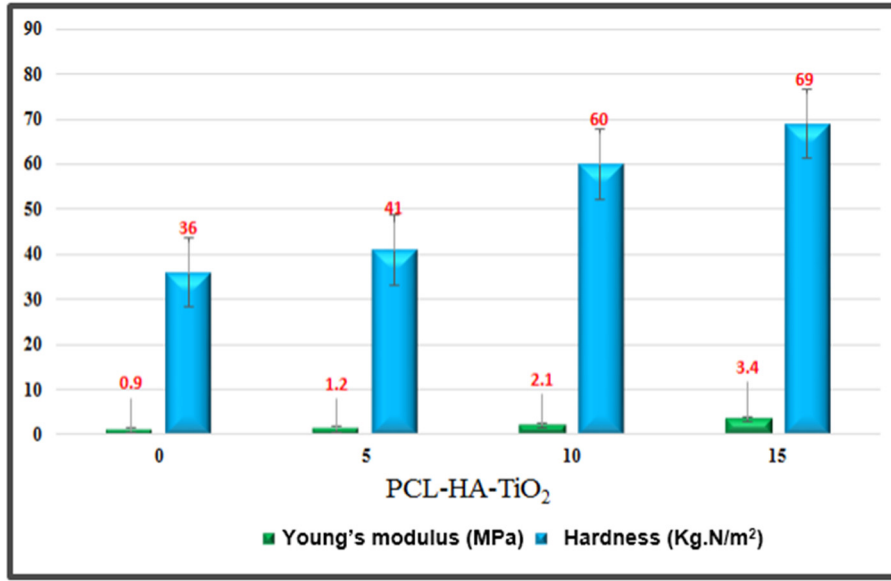


Fig.7. Hardness and Young's modulus diagram of PCL-HA-TiO₂

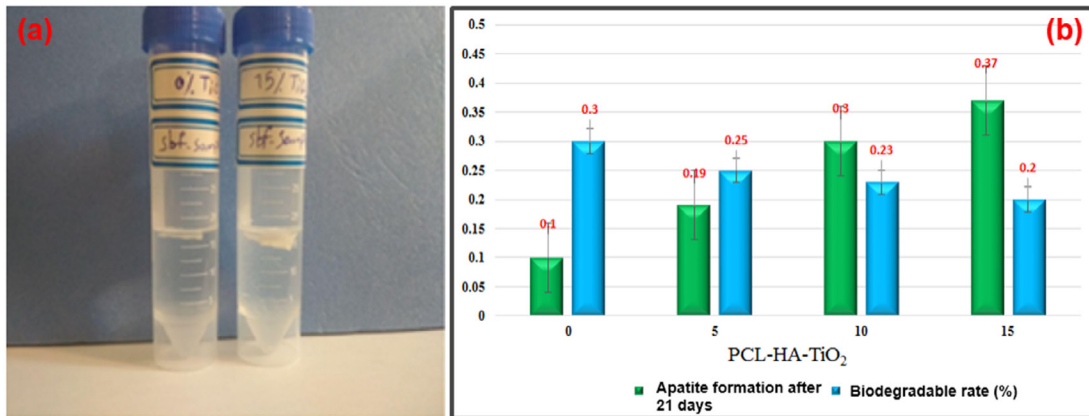


Fig.8. (a) Investigation of dissolution of 0 wt. % vs 15wt. % of TiO₂ (b) Apatite formation and biodegradable rate

Investigation of structure and phase determination of polymer / ceramic composites by XRD

The XRD spectra of HA, TiO₂, is shown in Fig (9). One of the reasons for XRD is to determine the percentage purity of the crystals. Pure HA crystals have a sharp peak of about 32-34 degrees, and pure TiO₂ crystal has a sharp peak of about 22-25 degrees. Figure (9) shows the XRD spectroscopy of 3D nanocomposite scaffolds. It is observed that pure HA (a) does not show any peak dispersion in the range of 10 to 22 degrees of 2θ. However, the above sample shows a series of peaks around 25 degrees, 26 degrees, 29 degrees, 36 degrees, 38 Shows 45 degrees, 47 degrees, 52 degrees, and 67

degrees. Sahmani et al., [47] the addition of MgO nanoparticles to the hydroxyapatite was consider using space holder technique including ibuprofen free surface coating. The samples presented proper mechanical and chemical properties through addition of MgO elements. Also, addition of magnetite nanoparticles to the bioglass was evaluated by Salmani et al. [48]

These peaks confirm the presence of a HA crystal lattice throughout the nanocomposite. And then there are several peaks for TiO₂ (b) around 25 degrees, 32 degrees, 35 degrees, 41 degrees, 49 degrees, 55 degrees, 64 degrees, 70 degrees, 75 degrees, and 85 degrees, hence this peak confirms

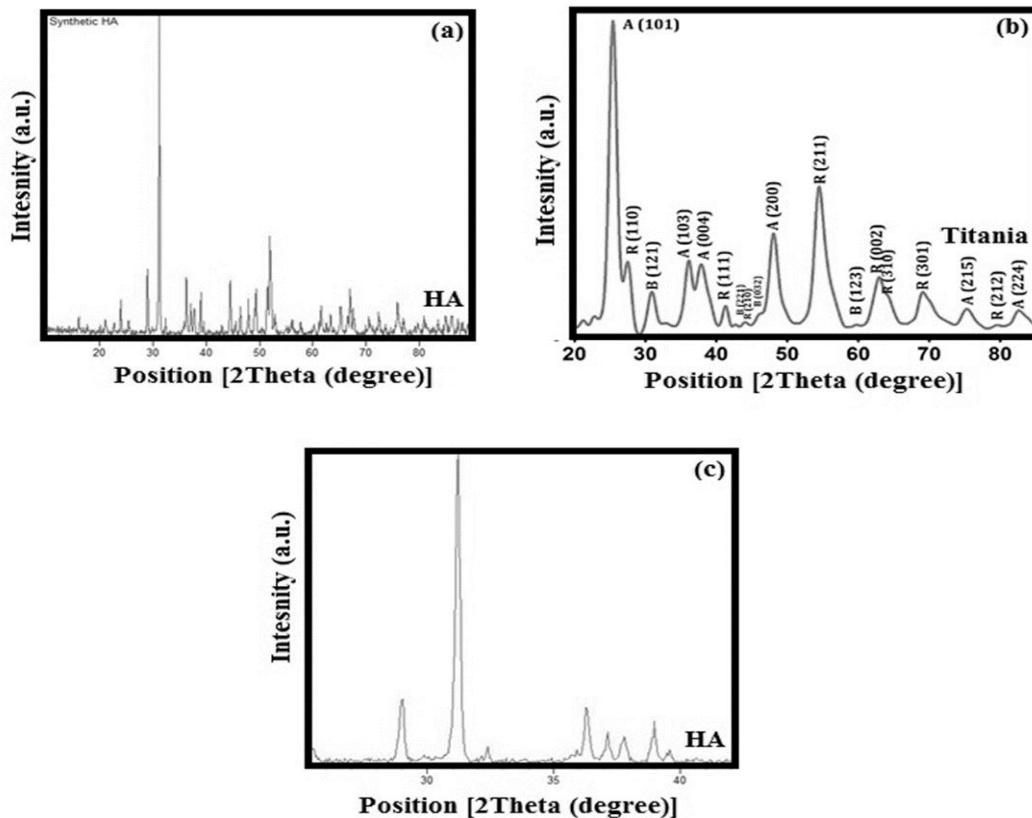


Fig.9. XRD pattern of consumable nanoparticles (a) Crystalline HA nanoparticles, (b) TiO_2 nanoparticles (c) Sharp peaks in HA nanoparticles

the presence of TiO_2 crystal lattice throughout the nanocomposite. Figure 3 (c) clearly shows the presence of a sharp peak of about 32 degrees, which indicates the highest crystalline state of HA nanoparticle at this degree.

Investigation of morphology and structure of composite scaffolds using SEM

SEM images well show the porosity created in the scaffolding. As can be seen, the pores are interconnected, and with the help of internal communication with each other can help significantly in trapping the drug. The walls of these pores are composed of PCL-HA- TiO_2 nanocomposites. The amount of HA nanoparticles directly affects the morphology of the scaffold. In Fig (10a) PCL polymer layers of nanocomposites (0 wt%-5wt%-10wt%-15wt% of TiO_2) are layered. In Fig (10b-c) the spherical spheres of HA nanoparticles are attached to the polymer layers, on which these spherical spheres of TiO_2 nanoparticles are placed as a reinforcement. Figure (10d) shows

the formation of TiO_2 nanoparticles on HA spheres. Fig (11) shows the formation of a titanium coating on HA nanoparticles.

Investigation of structural results using AFM spectroscopy

In surface studies of nanocomposite samples to investigate the relationship between hardness and roughness of the samples, the results of structural and microscopic examination of the samples showed that the addition of TiO_2 increased surface roughness of the samples. Advantages such as high active surface area, high reactivity, and insulating properties allow the application of these compounds in the field of soft and hard bone tissue engineering. The interaction of cavities with host molecules can be investigated based on supermolecular chemistry. By controlling the physicochemical environment of cavities, new properties can be provided in the interaction with guest molecules and the structure can be optimized for further applications. In Fig (12), images were taken from samples of (0, 5, 10 and, 15 wt. % of TiO_2) with

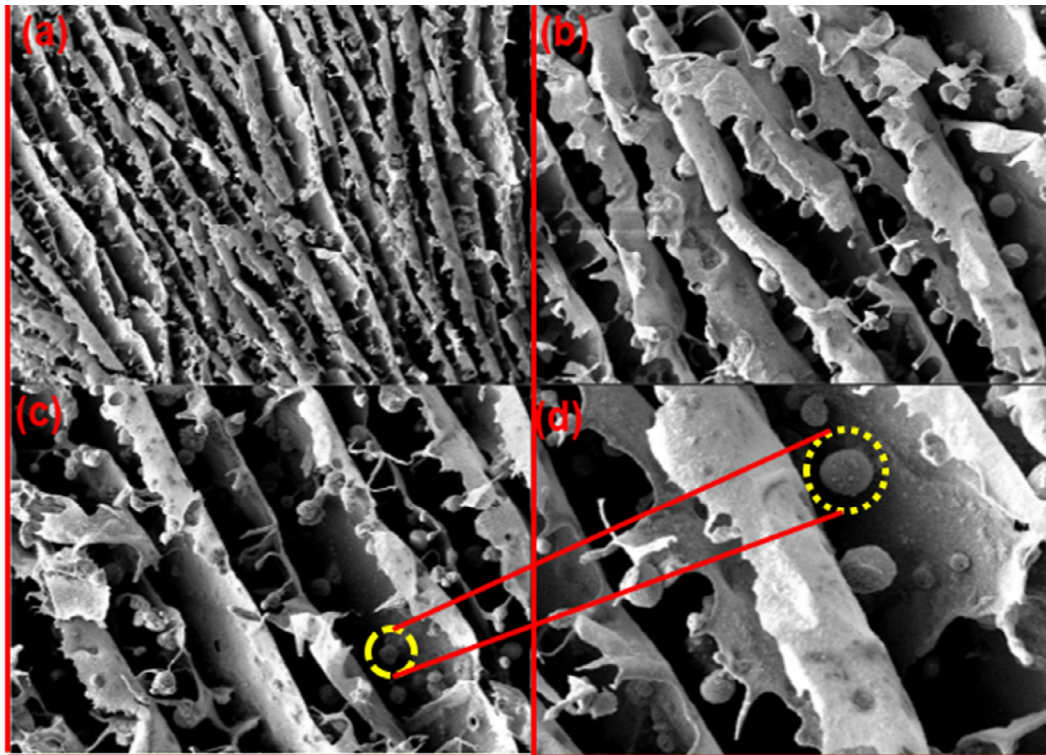


Fig.10. SEM image of a nanocomposite scaffold containing (a) 0, (b) 5, (c) 10, (d) 15 wt.% of TiO_2 in PCL matrix with scale of 10 to 100 microns

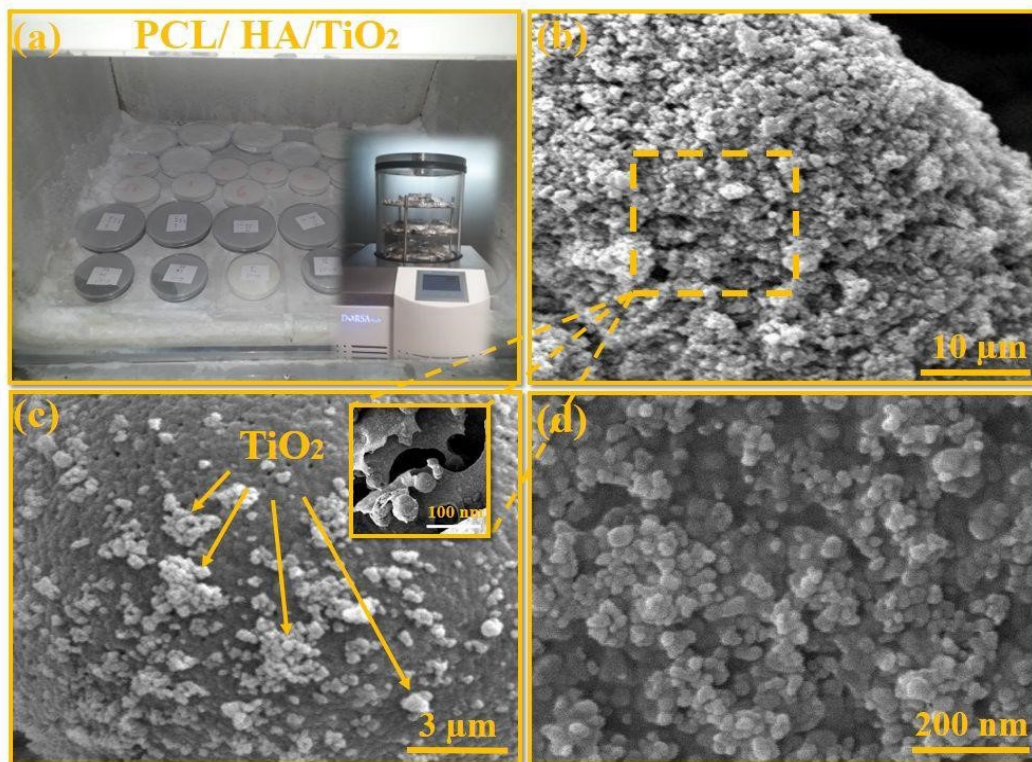


Fig.11. SEM image of a sample nanocomposite scaffold containing different weight percentages of titanium dioxide (0, 5, 10 and 15 wt. % of TiO_2)

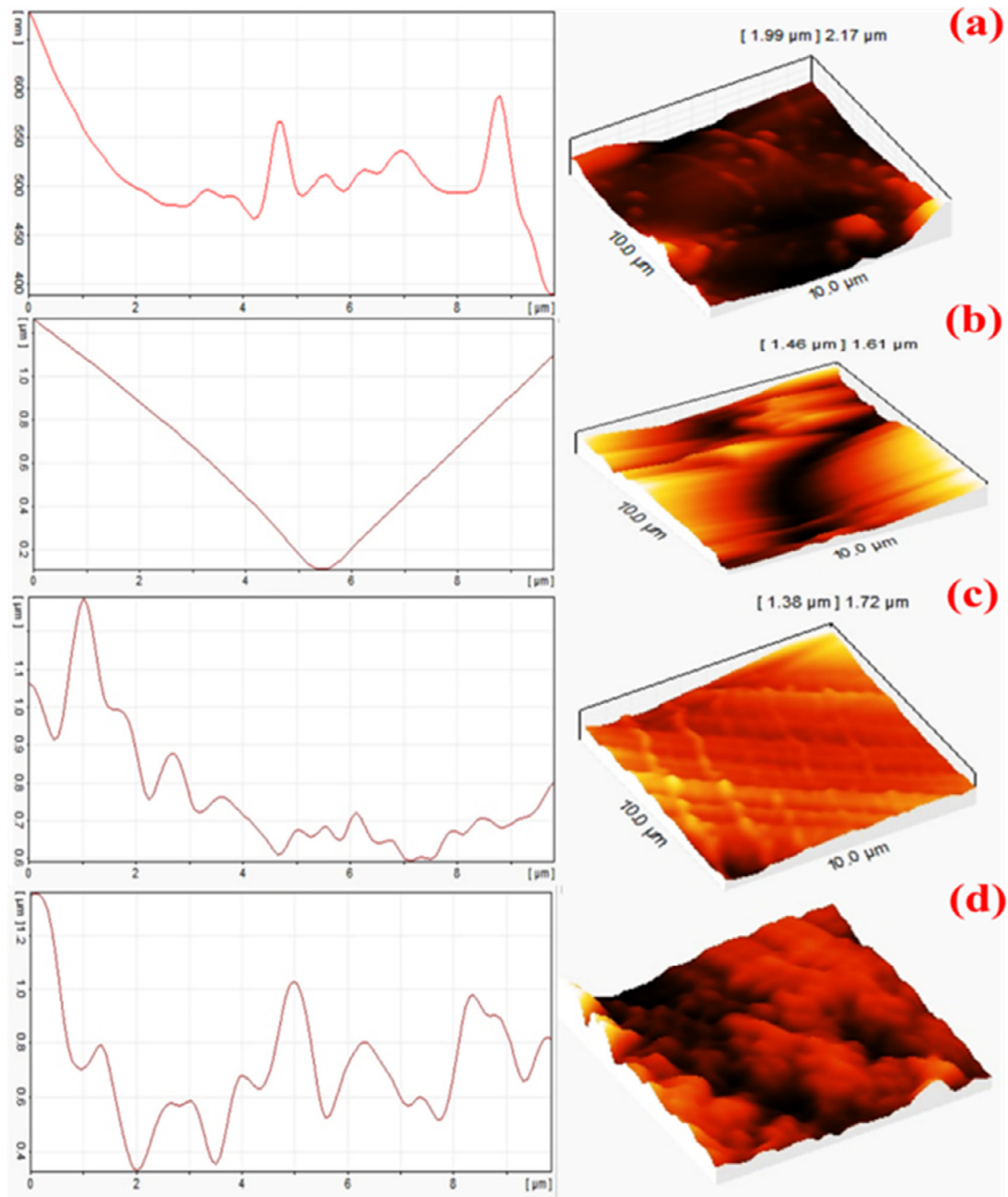


Fig.12. AFM analysis of the fabricated PCL-HA-TiO₂ porous bio-nanocomposites containing (a) 0 % wt, (b) 5 % wt, (c) 10 % wt, and (d) 15 % wt of TiO₂ within the scale of 5 to 10 microns

a length and width of between 5 to 10 microns, then their diagrams of each surface were drawn. The AFM image results show that the addition of TiO₂ increases the porosity of the surface of nanocomposite samples.

The size analysis of using HRTEM

In Fig. 13, nanospheres that are enclosed by

porous HA walls. In the images, the dark spots on the nanospheres' surface indicate the presence of TiO₂ nanoparticles, which are neatly positioned both on the surface and inside the nanospheres. The TiO₂ particles (the dark spots) have a size of about 40 nm, as observed in the HRTEM test.

The swelling properties of the prepared scaffolds

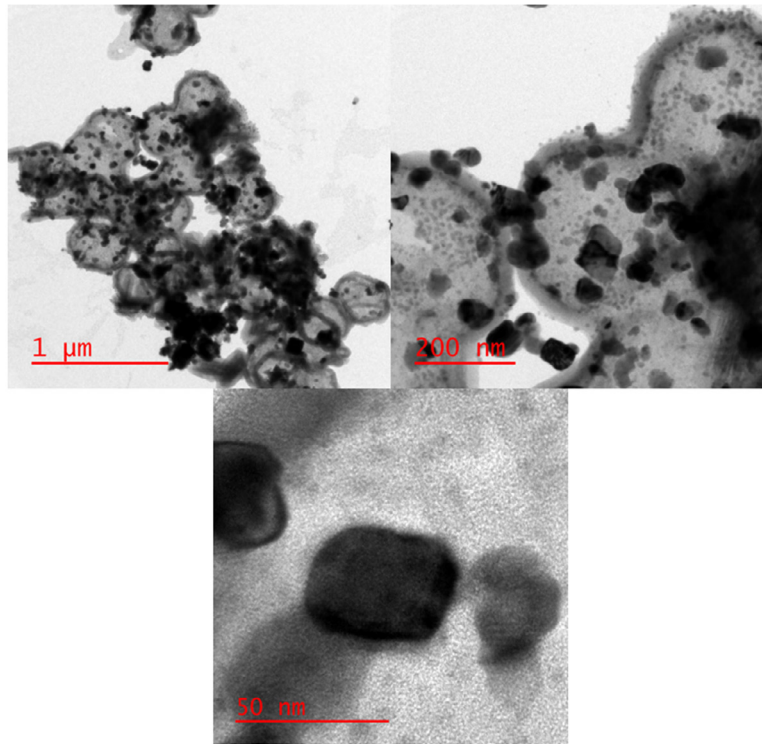


Fig. 13. HRTEM of nanospheres surrounded by porous HA walls

in PBS and SBF were investigated. For this purpose, bio-nanocomposites (0, 5, 10, 15, and 20 wt. % of $\text{Ag}_2\text{O}/\text{SiO}_2$) were immersed in the above solutions for 14 days. A digital scale then measured the weight of the samples in wet and dry conditions. Simulated Body Fluid (SBF) is a solution with ion concentrations close to human blood plasma, which is maintained at the same mild pH and physiological temperature. Simulated Body Fluid should only be used for the biological evaluation of synthetic materials in vitro. Water absorption in wound dressings is one of the critical biological characteristics of these composite materials. For this purpose, nanocomposites made with different percentages of nanoparticles in approximate dimensions of one in 1×1 cm are cut and weighed and then immersed in a solution of distilled water and SBF at 37°C . Over time, the nanocomposites were removed from the solution regularly until equilibrium was reached and weighed after cleaning the surface water. The water absorption percentage was determined using the following equation 1.

$$\text{Swelling Ratio} = \frac{W_b - W_a}{W_a} \times 100 \quad (1)$$

Where W_b and W_a are swollen and dry sample weights, respectively.

To use the pH paper, a strip of paper appropriate to the estimated pH range for the solution must first be selected. Then immerse the paper in the test solution, and remove it after 2 seconds to change the color of the paper to determine the pH. Finally, we should compare the color of the paper with the color spectrum of its guide to determine the pH of the solution.

Analysis of molecular dynamics simulation results

In this part, the mechanical properties including (Young's modulus and Poisson's ratio), and the physical properties including (density) of pure material are simulated. Nanocomposite boxes ($\text{HA-TiO}_2\text{-PCL}$) with (0, 5, 10, 15 wt% of TiO_2) are calculated as shown in Fig. 11. To simulate porous nanocomposite in MDs software, the total weight percent of HA and TiO_2 was 25% of the total weight and constant amount (75%) for the polymer. It should be noted that the overall weight of the composite is considered to be 8 gr, and the weight of the polymer (PCL) is considered 6 gr. All molecular details of the four case studies have been shown in Table 2.

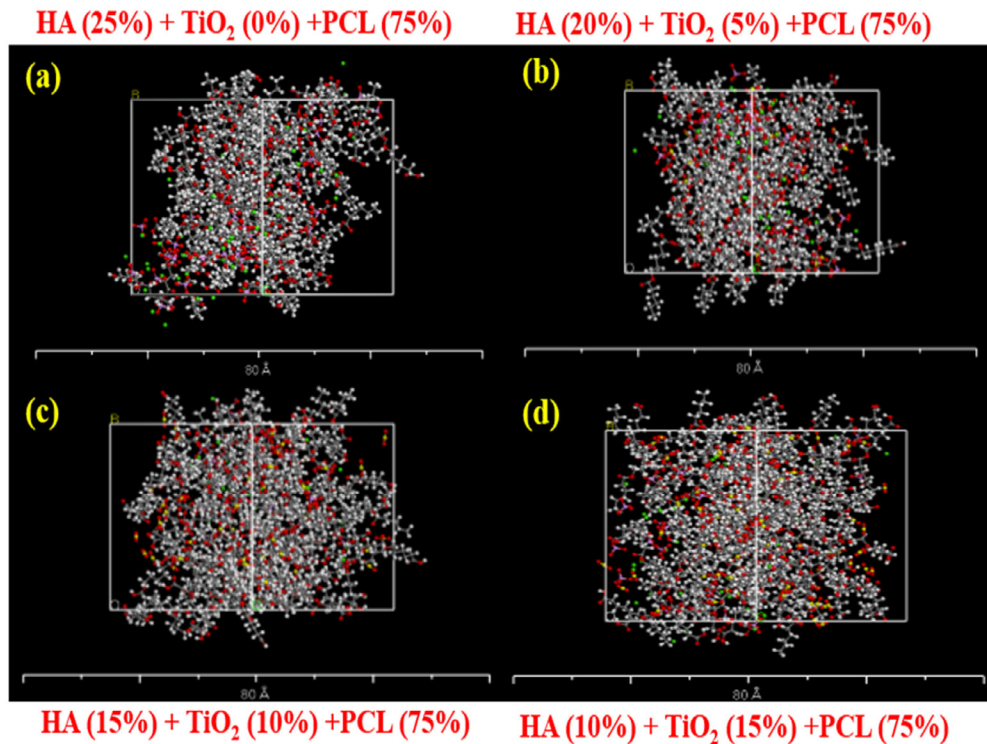


Fig.14. Simulation of (a): 0 wt%, (b): 5 wt %, (c): 10 wt%, (d): 15 wt% of TiO₂ with HA and PCL simulated in the Materials studio software

Table 2. Details of five case studies using (HA) and (TiO₂) as reinforcements

Description	Mass of matrix and reinforcements (gr)			Volume fraction of matrix and reinforcements (%)			No. of atoms	Lattice dimensions (Å°)
	TiO ₂	HA	PCL	TiO ₂	HA	PCL		
0 wt.% TiO ₂	0	2	6	0	25	75	2900	33.2×33.2×33.2
5wt.% TiO ₂	0.4	1.6	6	5	20	75	2960	33.9×33.9×33.9
10wt.% TiO ₂	0.8	1.2	6	10	15	75	3383	34.4×34.4×34.4
15wt.% TiO ₂	1.2	0.8	6	15	10	75	3848	36.1×36.1×36.1

The swelling properties of the prepared scaffolds in PBS and SBF were investigated. For this purpose, bio-nanocomposites (0wt. %, 5wt. %, 10wt. %, 15wt. % NPs) were immersed in the above solutions for 14 days. A digital scale then measured the weight of the samples in wet and dry conditions. Simulated Body Fluid (SBF) is a solution with ion concentrations close to human blood plasma, which is maintained at the same mild pH and physiological temperature. Simulated Body Fluid should only be used for the biological evaluation of synthetic materials in vitro. Water absorption in wound dressings is one of the critical biological characteristics of these composite materials. For this purpose, nanocomposites made with different percentages of nanoparticles in approximate dimensions of one in 1×1 cm are cut

and weighed and then immersed in a solution of distilled water and SBF at 37 ° C. Over time, the nanocomposites were removed from the solution regularly until equilibrium was reached and weighed after cleaning the surface water. The water absorption percentage was determined using the following equation 2.

$$Swelling\ Ratio = \frac{W_b - W_a}{W_a} \times 100 \quad (2)$$

Where W_b and W_a are swollen and dry sample weights, respectively.

To use the pH paper, a strip of paper appropriate to the estimated pH range for the solution must

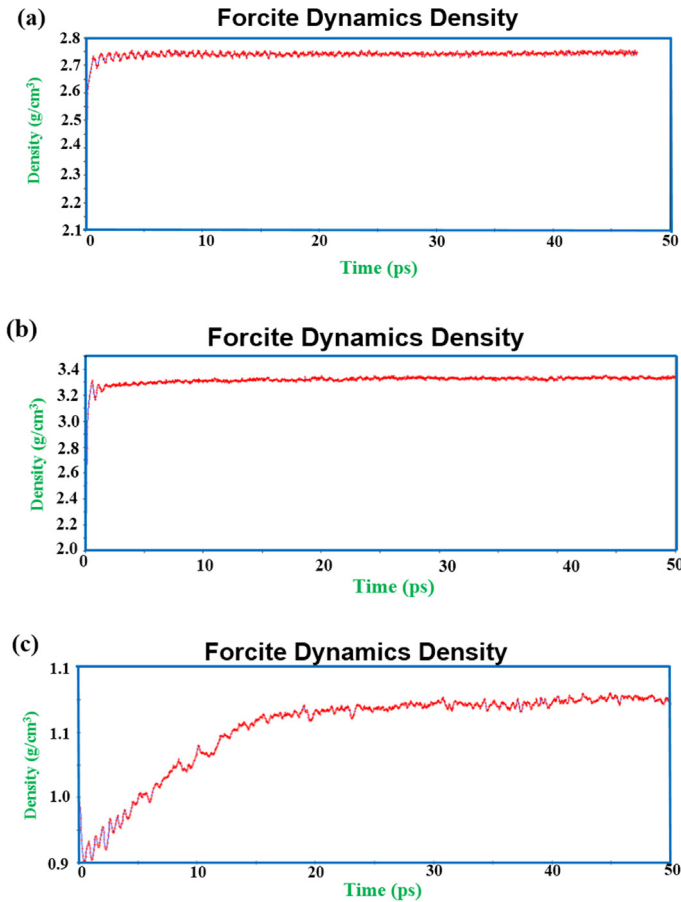


Fig.15. Density convergence during simulation for pure materials (a): HA (b): TiO₂ (c): PCL at the temperature of 298 °K

first be selected. Then immerse the paper in the test solution, and remove it after 2 seconds to change the color of the paper to determine the pH. Finally, we should compare the color of the paper with the color spectrum of its guide to determine the pH of the solution.

Results of MDs for pure materials

The mechanical and physical properties of (HA-TiO₂-PCL) are shown in (see Fig. (15), and Table 3) that by following the steps that mentioned in section 2.8 are derived the mechanical and physical properties. To draw the density diagram, first, the simulated NVT to maximize the energy of system and then the NPT was plotted to show the density. Table 3 shows the comparison of mechanical and physical properties of (HA-TiO₂-PCL) with molecular dynamics modeling and experimental analysis.

To reduce the diagrams, all properties of simulated nanocomposites are presented in Table 3.

To validate the simulation results, elastic stiffness matrix and elastic constants of the nanocomposite were determined using a constant strain method. The elastic stiffness matrix components were defined for (0, 5, 10, and 15wt. % of TiO₂) respectively, under a strain of 60.003 and at a pressure of 1 atm. These results are as follows:

$$C_{ij}(GPa) = \begin{bmatrix} 161.72 & 101.67 & 70.87 & 1.31 & -0.009 & 6.68 \\ 101.67 & 138.69 & 57.24 & 1.23 & 0.007 & 7.43 \\ 70.87 & 52.24 & 163.28 & 5.26 & -0.006 & 16.53 \\ 1.31 & 1.23 & 5.26 & 3.21 & 13.25 & -1.65 \\ -0.009 & 0.007 & -0.006 & 13.25 & 9.12 & 2.61 \\ 6.68 & 7.43 & 16.53 & -1.65 & 2.61 & 16.69 \end{bmatrix} \quad (2)$$

$$C_{ij}(GPa) = \begin{bmatrix} 193.49 & 64.96 & 70.72 & 0.001 & -8.27 & 0.01 \\ 64.96 & 200.10 & 68.60 & -0.003 & -9.51 & 0.01 \\ 70.72 & 68.60 & 225.18 & -0.004 & 10.83 & 0.002 \\ 0.001 & -0.003 & -0.004 & 50.12 & 0.004 & -6.12 \\ -8.27 & -9.51 & 10.83 & 0.004 & 31.28 & 0.01 \\ 0.01 & 0.01 & 0.002 & -6.12 & 0.01 & 42.54 \end{bmatrix} \quad (3)$$

Table 3. Compare of experimental and simulation test and obtaining percent error for (HA-TiO₂-PCL)

Mechanical properties	References	Simulation (MDs)	Percent error (%)
Young's Modulus of pure HA (GPa)	6 [49]	5.75	4.16
Poisson's ratio of pure HA	0.27 [50]	0.26	3.7
Young's Modulus of pure TiO ₂ (GPa)	230 [51]	222	3.47
Poisson's ratio of pure TiO ₂	0.27 [52]	0.25	7.40
Young's Modulus of pure PCL (GPa)	1.2	1.18	1.67
Poisson's ratio of pure PCL	0.30	0.28	6.66

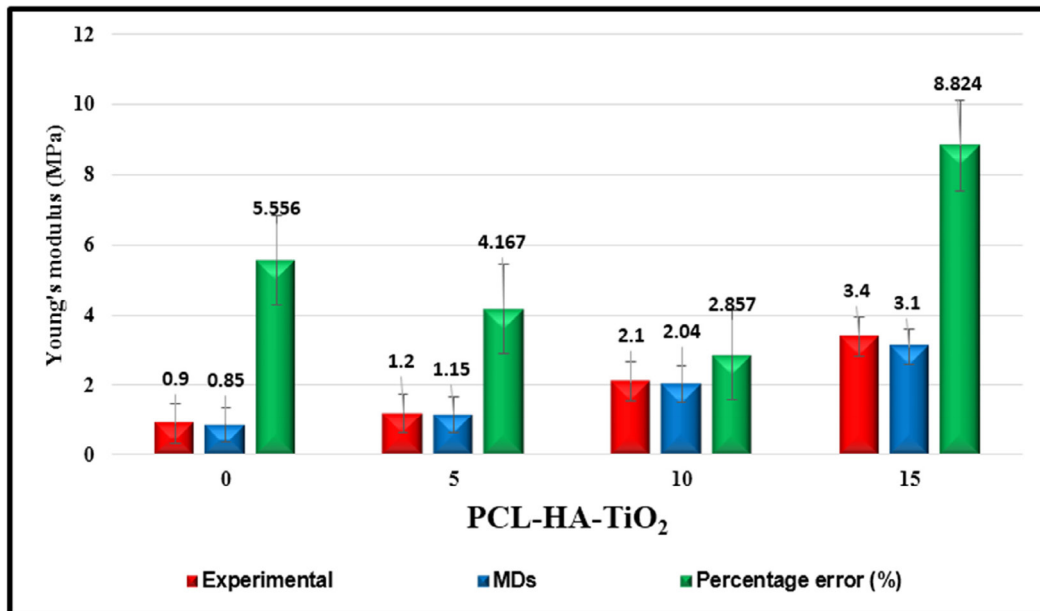


Fig.16. Comparison of Young's modulus of fabricated and simulated nanocomposites by two methods of (experimental and MDs)

$$C_{ij}(GPa) = \begin{bmatrix} 7.32 & 0.11 & -0.15 & -0.24 & -2.05 & -0.34 \\ 0.11 & 3.02 & 4.96 & -0.97 & 2.10 & 1.16 \\ -0.15 & 4.96 & 4.42 & -2.19 & 4.22 & 3.52 \\ -0.24 & -0.97 & -2.19 & 1.76 & -0.68 & -0.68 \\ -2.05 & 2.10 & 4.22 & -0.68 & 4.13 & 1.29 \\ -0.34 & 1.16 & 3.53 & -0.68 & 1.29 & 7.31 \end{bmatrix} \quad (4)$$

$$C_{ij}(GPa) = \begin{bmatrix} 3.86 & 186.82 & 182.96 & -0.12 & 2.75 & 4.78 \\ 186.82 & 2.008 & 3.05 & -0.22 & 0.006 & 0.008 \\ 182.96 & 3.05 & 7.31 & 0.78 & -0.40 & 0.02 \\ -0.12 & -0.22 & 0.789 & 0.31 & 0.02 & 0.67 \\ 2.750 & 0.006 & -0.40 & 0.02 & 0.39 & 0.42 \\ 4.78 & 0.008 & 0.023 & 0.67 & 0.42 & 0.50 \end{bmatrix} \quad (5)$$

As can be observed, because of the isotropy of the material, the diagonal elements are nearly similar and the matrix is approximately symmetric. In this paper, Young's modulus diagram obtained by the laboratory method and MDs method for all four composites (0, 5, 10, 15 wt. % of TiO₂) is compared with each other as shown in Fig (16).

CONCLUSION

In this paper, bio-nanocomposites fabricated and simulated with different weight percentages (0 wt. %, 5wt. %, 10wt. %, 15wt. %) of TiO₂ by both

experimental and MDs methods. The fabrication of this nanocomposite is significantly effective for bone fusion as well as for bone implants. The novelty of this research compared to other researches are mixed biological materials in experimental and simulation together and calculated with the least error. The main results of this research are:

- With the increase of TiO₂ nanoparticles, the fracture toughness increases up to 10 wt. % of TiO₂ and then decreases.
- As the TiO₂ nanoparticles increase, the hardness of the fabricated nanocomposite increases.
- The Young's modulus increases with the increase of TiO₂ nanoparticles.
- With increasing TiO₂ nanoparticles, the porosity of the nanocomposites increases.
- As TiO₂ nanoparticles increases, the process of apatite formation increases approximately threefold, and the dissolution rate decreases with increasing TiO₂.
- The percentage of errors in the experimental sample and the predicted values in the MDs method were very small and close to each other, which indicates the accuracy of this method.

ACKNOWLEDGMENT

The authors are thankful to the Iranian Nanotechnology Development Committee for their support.

FUNDING

The authors received no financial support for the research, authorship, and publication of this article.

AVAILABILITY OF DATA AND MATERIALS

Data required to reproduce these findings have been given in the text.

REFERENCES

- [1] D. Dippold, M. Tallawi, S. Tansaz, J.A. Roether, A.R. Boccaccini, Novel electrospun poly(glycerol sebacate)-zein fiber mats as candidate materials for cardiac tissue engineering, *Eur. Polym. J.* 75 (2016) 504-513. <https://doi.org/10.1016/j.eurpolymj.2015.12.030>
- [2] A. Salerno, L. Verdolotti, M.G. Raucci, J. Saurina, C. Domingo, R. Lamanna, V. Iozzino, M. Lavorgna, Hybrid gelatin-based porous materials with a tunable multiscale morphology for tissue engineering and drug delivery, *Eur. Polym. J.* 99 (2018) 230-239. <https://doi.org/10.1016/j.eurpolymj.2017.12.024>
- [3] A. Farzan, S. Borandeh, N. Zanjanizadeh Ezazi, S. Lipponen, H.A. Santos, J. Seppälä, 3D scaffolding of fast photocurable polyurethane for soft tissue engineering by stereolithography: Influence of materials and geometry on growth of fibroblast cells, *Eur. Polym. J.* 139 (2020) 109988. <https://doi.org/10.1016/j.eurpolymj.2020.109988>
- [4] M. Rostamian, M.R. Kalae, S.R. Dehkordi, M. Panahi-Sarmad, M. Tirgar, V. Goodarzi, Design and characterization of poly(glycerol-sebacate)-copoly(caprolactone) (PGS-co-PCL) and its nanocomposites as novel biomaterials: The promising candidate for soft tissue engineering, *Eur. Polym. J.* 138 (2020) 109985. <https://doi.org/10.1016/j.eurpolymj.2020.109985>
- [5] A. Eyvazian, C. Zhang, F. Musharavati, A. Farazin, M. Mohammadimehr, A. Khan, Effects of appearance characteristics on the mechanical properties of defective SWCNTs: using finite element methods and molecular dynamics simulation, *Eur. Phys. J. Plus.* 136 (2021) 946. <https://doi.org/10.1140/epjp/s13360-021-01840-y>
- [6] S. Tavasolikejani, A. Farazin, Explore the most recent advancements in the domain of self-healing intelligent composites specifically designed for use in dentistry, *J. Mech. Behav. Biomed. Mater.* (2023) 106123. <https://doi.org/10.1016/j.jmbbm.2023.106123>
- [7] M. Hassan, K. Dave, R. Chandrawati, F. Dehghani, V.G. Gomes, 3D printing of biopolymer nanocomposites for tissue engineering: Nanomaterials, processing and structure-function relation, *Eur. Polym. J.* 121 (2019) 109340. <https://doi.org/10.1016/j.eurpolymj.2019.109340>
- [8] N. Dehghan-Manshadi, S. Fattahi, M. Hadizadeh, H. Nikukar, S.M. Moshtaghioun, B. Aflatoonian, The influence of elastomeric polyurethane type and ratio on the physicochemical properties of electrospun polyurethane/silk fibroin hybrid nanofibers as potential scaffolds for soft and hard tissue engineering, *Eur. Polym. J.* 121 (2019) 109294. <https://doi.org/10.1016/j.eurpolymj.2019.109294>
- [9] R. Mishra, R. Varshney, N. Das, D. Sircar, P. Roy, Synthesis and characterization of gelatin-PVP polymer composite scaffold for potential application in bone tissue engineering, *Eur. Polym. J.* 119 (2019) 155-168. <https://doi.org/10.1016/j.eurpolymj.2019.07.007>
- [10] A. Emami, T. Talaei-Khozani, Z. Vojdani, N. Zarei fard, Comparative assessment of the efficiency of various decellularization agents for bone tissue engineering, *J. Biomed. Mater. Res. Part B Appl. Biomater.* 109 (2021) 19-32. <https://doi.org/10.1002/jbm.b.34697>
- [11] A. Kumar, S.M. Mir, I. Aldulijan, A. Mahajan, A. Anwar, C.H. Leon, A. Terracciano, X. Zhao, T. Su, D.M. Kalyon, S.G. Kumbar, X. Yu, Load-bearing biodegradable PCL-PGA-beta TCP scaffolds for bone tissue regeneration, *J. Biomed. Mater. Res. Part B Appl. Biomater.* 109 (2021) 193-200. <https://doi.org/10.1002/jbm.b.34691>
- [12] A. Alijagic, F. Barbero, D. Gaglio, E. Napodano, O. Benada, O. Kofroňová, V.F. Puentes, N.G. Bastús, A. Pinsino, Gold nanoparticles coated with polyvinylpyrrolidone and sea urchin extracellular molecules induce transient immune activation, *J. Hazard. Mater.* 402 (2021) 123793. <https://doi.org/10.1016/j.jhazmat.2020.123793>
- [13] A. Farazin, M. Mohammadimehr, H. Naeimi, Flexible self-healing nanocomposite based gelatin/tannic acid/acrylic acid reinforced with zinc oxide nanoparticles and hollow silver nanoparticles based on porous silica for rapid wound healing, *Int. J. Biol. Macromol.* 241 (2023) 124572. <https://doi.org/10.1016/j.ijbiomac.2023.124572>
- [14] A. Farazin, F.A. Shirazi, M. Shafei, Natural biomarocmoleculu-based antimicrobial hydrogel for rapid wound healing: A review, *Int. J. Biol. Macromol.* 244 (2023)

125454. <https://doi.org/10.1016/j.ijbiomac.2023.125454>
- [15] A. Farazin, C. Zhang, A.H. Ghasemi, Preparation and identification of new antibacterial and biocompatible dressings based on gelatin/polyvinyl alcohol and castor oil, *J. Polym. Res.* 30 (2023) 125. <https://doi.org/10.1007/s10965-023-03505-z>
- [16] A. Farazin, C. Zhang, A. Gheisizadeh, A. Shahbazi, 3D bio-printing for use as bone replacement tissues: A review of biomedical application, *Biomed. Eng. Adv.* 5 (2023) 100075. <https://doi.org/10.1016/j.bea.2023.100075>
- [17] A. Ghorbanpour Arani, N. Miralaei, A. Farazin, M. Mohammadimehr, An extensive review of the repair behavior of smart self-healing polymer matrix composites, *J. Mater. Res.* 38 (2023) 617-632. <https://doi.org/10.1557/s43578-022-00884-9>
- [18] A. Farazin, A.H. Ghasemi, Design, Synthesis, and Fabrication of Chitosan/Hydroxyapatite Composite Scaffold for Use as Bone Replacement Tissue by Sol-Gel Method, *J. Inorg. Organomet. Polym. Mater.* 32 (2022) 3067-3082. <https://doi.org/10.1007/s10904-022-02343-8>
- [19] L.P. da Silva, S.C. Kundu, R.L. Reis, V.M. Correlo, Electric Phenomenon: A Disregarded Tool in Tissue Engineering and Regenerative Medicine, *Trends Biotechnol.* 38 (2020) 24-49. <https://doi.org/10.1016/j.tibtech.2019.07.002>
- [20] C.D. Spicer, Hydrogel scaffolds for tissue engineering: the importance of polymer choice, *Polym. Chem.* 11 (2020) 184-219. <https://doi.org/10.1039/C9PY01021A>
- [21] N. Johari, L. Moroni, A. Samadikuchaksaraei, Tuning the conformation and mechanical properties of silk fibroin hydrogels, *Eur. Polym. J.* 134 (2020) 109842. <https://doi.org/10.1016/j.eurpolymj.2020.109842>
- [22] P. Naderi, M. Zarei, S. Karbasi, H. Salehi, Evaluation of the effects of keratin on physical, mechanical and biological properties of poly (3-hydroxybutyrate) electrospun scaffold: Potential application in bone tissue engineering, *Eur. Polym. J.* 124 (2020) 109502. <https://doi.org/10.1016/j.eurpolymj.2020.109502>
- [23] V.A. Reyna-Urrutia, V. Mata-Haro, J. V. Cauich-Rodriguez, W.A. Herrera-Kao, J.M. Cervantes-Uc, Effect of two crosslinking methods on the physicochemical and biological properties of the collagen-chitosan scaffolds, *Eur. Polym. J.* 117 (2019) 424-433. <https://doi.org/10.1016/j.eurpolymj.2019.05.010>
- [24] C. Zhang, P. Dong, Y. Bai, D. Quan, Nanofibrous polyester-peptide block copolymer scaffolds with high porosity and controlled degradation promote cell adhesion, proliferation and differentiation, *Eur. Polym. J.* 130 (2020) 109647. <https://doi.org/10.1016/j.eurpolymj.2020.109647>
- [25] B. Naton, M. Ecke, R. Hampp, Production of fertile hybrids by electrofusion of vacuolated and evacuated tobacco mesophyll protoplasts, *Plant Sci.* 85 (1992) 197-208. [https://doi.org/10.1016/0168-9452\(92\)90116-4](https://doi.org/10.1016/0168-9452(92)90116-4)
- [26] M. Haghghi, A. Khodadadi, H. Golestanian, F. Aghadavoudi, Effects of defects and functional groups on graphene and nanotube thermoset epoxy-based nanocomposites mechanical properties using molecular dynamics simulation, *Polym. Polym. Compos.* (2020) 096739112092907. <https://doi.org/10.1177/0967391120929075>
- [27] A. Montazeri, M. Sadeghi, R. Naghdabadi, H. Raffi-Tabar, Multiscale modeling of the effect of carbon nanotube orientation on the shear deformation properties of reinforced polymer-based composites, *Phys. Lett. A.* 375 (2011) 1588-1597. <https://doi.org/10.1016/j.physleta.2011.02.065>
- [28] B. Mortazavi, G. Cuniberti, T. Rabczuk, Mechanical properties and thermal conductivity of graphitic carbon nitride: A molecular dynamics study, *Comput. Mater. Sci.* 99 (2015) 285-289. <https://doi.org/10.1016/j.commatsci.2014.12.036>
- [29] S.-P. Ju, C.-C. Chen, T.-J. Huang, C.-H. Liao, H.-L. Chen, Y.-C. Chuang, Y.-C. Wu, H.-T. Chen, Investigation of the structural and mechanical properties of polypropylene-based carbon fiber nanocomposites by experimental measurement and molecular dynamics simulation, *Comput. Mater. Sci.* 115 (2016) 1-10. <https://doi.org/10.1016/j.commatsci.2015.12.032>
- [30] S. Frankland, The stress-strain behavior of polymer-nanotube composites from molecular dynamics simulation, *Compos. Sci. Technol.* 63 (2003) 1655-1661. [https://doi.org/10.1016/S0266-3538\(03\)00059-9](https://doi.org/10.1016/S0266-3538(03)00059-9)
- [31] V. Marcadon, D. Brown, E. Hervé, P. Mélé, N.D. Albréra, A. Zaoui, Confrontation between Molecular Dynamics and micromechanical approaches to investigate particle size effects on the mechanical behaviour of polymer nanocomposites, *Comput. Mater. Sci.* 79 (2013) 495-505. <https://doi.org/10.1016/j.commatsci.2013.07.002>
- [32] Y. Han, J. Elliott, Molecular dynamics simulations of the elastic properties of polymer/carbon nanotube composites, *Comput. Mater. Sci.* 39 (2007) 315-323. <https://doi.org/10.1016/j.commatsci.2006.06.011>
- [33] A.R.C. Baljon, M.O. Robbins, Simulations of Crazing in Polymer Glasses: Effect of Chain Length and Surface Tension, *Macromolecules.* 34 (2001) 4200-4209. <https://doi.org/10.1021/ma0012393>
- [34] P.K. Naicker, P.T. Cummings, H. Zhang, J.F. Banfield, Characterization of Titanium Dioxide Nanoparticles Using Molecular Dynamics Simulations, *J. Phys. Chem. B.* 109 (2005) 15243-15249. <https://doi.org/10.1021/jp050963q>
- [35] H. Zhang, X. Lu, Y. Leng, L. Fang, S. Qu, B. Feng, J. Weng, J. Wang, Molecular dynamics simulations on the interaction between polymers and hydroxyapatite with and without coupling agents, *Acta Biomater.* 5 (2009) 1169-1181. <https://doi.org/10.1016/j.actbio.2008.11.014>
- [36] R.G. Forlong, Focal point characteristics and habitat use curves of underyearling brown trout (*Salmo trutta*) in the Kahuterawa Stream: a thesis presented in partial fulfilment of the requirements for the degree of Master of Science in Zoology at Massey University, (1988).
- [37] T. Kokubo, H. Takadama, How useful is SBF in predicting in vivo bone bioactivity?, *Biomaterials.* 27 (2006) 2907-2915. <https://doi.org/10.1016/j.biomaterials.2006.01.017>
- [38] K. Kalantari, E. Mostafavi, B. Saleh, P. Soltantabar, T.J. Webster, Chitosan/PVA hydrogels incorporated with green synthesized cerium oxide nanoparticles for wound healing applications, *Eur. Polym. J.* 134 (2020) 109853. <https://doi.org/10.1016/j.eurpolymj.2020.109853>
- [39] W. Miao, W. Zou, Y. Luo, N. Zheng, Q. Zhao, T. Xie, Structural tuning of polycaprolactone based thermadap shape memory polymer, *Polym. Chem.* 11 (2020) 1369-1374. <https://doi.org/10.1039/C9PY01891C>
- [40] A.A. Menazea, S.A. Abdelbadie, M.K. Ahmed, Manipulation of AgNPs coated on selenium/carbonated hydroxyapatite/ε-polycaprolactone nano-fibrous via pulsed laser deposition for wound healing applications, *Appl. Surf. Sci.* 508 (2020) 145299. <https://doi.org/10.1016/j>

- apsusc.2020.145299
- [41] T.P. Ribeiro, F.J. Monteiro, M.S. Laranjeira, PEGylation of iron doped hydroxyapatite nanoparticles for increased applicability as MRI contrast agents and as drug vehicles: A study on thrombogenicity, cytocompatibility and drug loading, *Eur. Polym. J.* 137 (2020) 109934. <https://doi.org/10.1016/j.eurpolymj.2020.109934>
- [42] S. Guo, H. Yoshioka, Y. Kato, H. Kakehi, M. Miura, N. Isu, A. Manseri, H. Sawada, B. Ameduri, Photocatalytic activity of vinylidene fluoride-containing copolymers/anatase titanium oxide/silica nanocomposites, *Eur. Polym. J.* 58 (2014) 79-89. <https://doi.org/10.1016/j.eurpolymj.2014.04.022>
- [43] Y. Xing, L. Wang, H. Yu, A. Khan, F. Haq, L. Zhu, Recent progress in preparation of branched polyethylene with nickel, titanium, vanadium and chromium catalytic systems and EPR study of related catalytic systems, *Eur. Polym. J.* 121 (2019) 109339. <https://doi.org/10.1016/j.eurpolymj.2019.109339>
- [44] N. Politakos, E. Diamanti, S.E. Moya, Smart, biocompatible, responsive surfaces on pH, temperature and ionic strength of titanium oxide and niobium oxide with polymer brushes of poly(acrylic acid), poly(N-isopropylacrylamide) and poly([2-(methacryloyloxy)ethyl] trimethylammonium chloride), *Eur. Polym. J.* 112 (2019) 306-319. <https://doi.org/10.1016/j.eurpolymj.2019.01.018>
- [45] Y. Hu, Y. Shao, Z. Liu, X. He, B. Liu, Effect of short-chain branching on the tie chains and dynamics of bimodal polyethylene: Molecular dynamics simulation, *Eur. Polym. J.* 103 (2018) 312-321. <https://doi.org/10.1016/j.eurpolymj.2018.01.006>
- [46] L.G. Lascane, E.F. Oliveira, D.S. Galvão, A. Batagin-Neto, Polyfuran-based chemical sensors: Identification of promising derivatives via DFT calculations and fully atomistic reactive molecular dynamics, *Eur. Polym. J.* 141 (2020) 110085. <https://doi.org/10.1016/j.eurpolymj.2020.110085>
- [47] S. Sahmani, S. Saber-Samandari, A. Khandan, M.M. Aghdam, Influence of MgO nanoparticles on the mechanical properties of coated hydroxyapatite nanocomposite scaffolds produced via space holder technique: Fabrication, characterization and simulation, *J. Mech. Behav. Biomed. Mater.* 95 (2019) 76-88. <https://doi.org/10.1016/j.jmbbm.2019.03.014>
- [48] M.M. Salmani, M. Hashemian, H.J. Yekta, M.G. Nejad, S. Saber-Samandari, A. Khandan, Synergic Effects of Magnetic Nanoparticles on Hyperthermia-Based Therapy and Controlled Drug Delivery for Bone Substitute Application, *J. Supercond. Nov. Magn.* 33 (2020) 2809-2820. <https://doi.org/10.1007/s10948-020-05530-1>
- [49] D. Timpu, L. Sacarescu, T. Vasiliu, M.V. Dinu, G. David, Surface cationic functionalized nano-hydroxyapatite - Preparation, characterization, effect of coverage on properties and related applications, *Eur. Polym. J.* 132 (2020) 109759. <https://doi.org/10.1016/j.eurpolymj.2020.109759>
- [50] M.K. Ahmed, A.M. Moydeen, A.M. Ismail, M.E. El-Naggar, A.A. Menazea, M.H. El-Newehy, Wound dressing properties of functionalized environmentally biopolymer loaded with selenium nanoparticles, *J. Mol. Struct.* 1225 (2021) 129138. <https://doi.org/10.1016/j.molstruc.2020.129138>
- [51] A. Boonmahitthisud, S. Chuayjuljit, K. Kamhangdechpol, M. Polsranoi, Nanocomposites of high-impact polystyrene with unmodified nanosized TiO₂ and polystyrene-encapsulated MPTMS-modified nanosized TiO₂: mechanical, thermal and morphological properties, *Plast. Rubber Compos. (2020)* 1-9. <https://doi.org/10.1080/14658011.2020.1838710>
- [52] Q. Ibrahim, R. Akbarzadeh, A photocatalytic TiO₂/graphene bilayer membrane design for water desalination: a molecular dynamic simulation, *J. Mol. Model.* 26 (2020) 165. <https://doi.org/10.1007/s00894-020-04422-4>